Nascent morphology of syndiotactic polystyrene synthesized over silica-supported metallocene catalyst

Joong Jin Han [a], Won Jung Yoon [b], Hyung Woo Lee [a,1], Kyu Yong Choi [a,*]

[a] Department of Chemical and Biomolecular Engineering, University of Maryland, College Park, MD 20853, USA
[b] Department of Chemical Bioengineering, Kyungwon University, San 65 Bokjeong-dong, Sujeong-gu, Seongnam, Gyeonggi-do 461-701, Republic of Korea

ABSTRACT

The nascent morphology of semi-crystalline syndiotactic polystyrene (sPS) polymerized over silica-supported pentamethyl cyclopentadienyl titanium trimethoxide ($Cp^*Ti(OCH_3)_3$) catalyst in a liquid slurry polymerization has been investigated under various reaction conditions. The scanning electron microscopic analysis of nascent polymers reveals that sPS molecules grow as long nanofibrils of 30–50 nm diameter and X-ray diffraction analysis shows the co-crystalline phases including both sPS and low molecular weight guest molecules of monomer and diluent. The energy dispersive X-ray spectroscopy also shows that the disintegration of silica primary particles occurs during the polymerization as evidenced by the uniform dispersion of silicon and aluminum in a polymer particle. The fibrous growth of the polymer inside a polymer particle leads to the shape replication of the original silica particles.

© 2008 Elsevier Ltd. All rights reserved.

1. Introduction

Syndiotactic polystyrene (sPS) is a semi-crystalline polymer characterized by high melting point ($T_m = 270\ ^\circ C$), strong chemical resistance, good electrical insulating properties, low melt viscosity, excellent dimensional stability, and low moisture absorption [1,2]. Neat and glass-filled syndiotactic polystyrenes are used in automotive, electrical, and industrial parts. Since the synthesis of sPS was first reported by Ishihara et al. [3,4], many studies have been reported on the polymerization catalysts, polymerization kinetics, physical transition phenomena, and crystallization of sPS having four different crystalline forms (i.e., α, β, γ, δ forms) as well as several co-crystalline forms with low molecular weight guest molecules.

sPS can be synthesized over titanium-based homogeneous metallocene catalysts in conjunction with methyl aluminoxane co-catalyst (e.g., CpTiCl$_3$/MAO or $Cp^*Ti(OCH_3)_3$/MAO). The bulk polymerization of styrene to sPS is characterized by the precipitation and gelation of sPS that is insoluble in its own monomer or other common organic solvents at typical reaction temperature of 40–90 °C [5,6]. The sPS gel is not a covalently cross-linked gel but a thermoreversible gel with 2_1-helix conformation [7–9]. Once the global gelation occurs, mixing the reaction mixture with a conventional agitator becomes extremely difficult.

The global gelation can be avoided if a heterogenized catalyst is used in a slurry process. When styrene is polymerized to sPS over heterogeneous metallocene catalysts such as embedded catalyst or silica-supported catalyst, a series of complex phase changes occur during the polymerization [10]. At very low monomer conversion, the reaction mixture is a clear liquid with no visible particle precipitation. But as the total solid content (TSC) increases, precipitated polymer particles start to agglomerate and the reaction mixture becomes turbid. The polymer agglomerates are transformed to soft or low density aggregates which become larger as conversion increases. These polymer aggregates can absorb a large amount of solvent and monomer in the reactor. As TSC further increases, the amount of liquid (monomer and solvent) imbibed in the sPS particles increases such that the reaction mixture eventually becomes a wet cake or paste-like material [10]. In our previous work, we have shown that sPS can be recovered as discrete particles with heterogeneous $Cp^*Ti(OCH_3)_3$/MAO catalyst (e.g., embedded catalyst or silica-supported catalyst) if the polymerization conditions are also properly controlled [10,11].

Another interesting but important characteristic of sPS is that it exhibits complex polymorphic behavior of having four different crystalline forms (i.e., α, β, γ, δ forms). sPS chains can adopt two stable conformations: all-*trans* planar zigzag (*TTTT*) and 2_1-helix (*TTGG*). The *TTGG* conformation obtained for sPS in solution or after absorption of solvent molecules is believed to be responsible for the thermoreversible gelation of sPS [12–14]. For example, when a thin layer of sPS film is exposed to a liquid solvent such as chloroform, benzophenone, tetrahydrofuran (THF), 1,2-dichloroethane (DCE), and trichlorethane (TCE) at a temperature below the glass

* Corresponding author. Tel.: +1 301 405 1907; fax: +1 301 405 0523.
E-mail address: choi@umd.edu (K.Y. Choi).
[1] Present address: Pt. Garuda Twin Jaya, JL. Teuku Nyak Arief #10, Jakarta 12220, Indonesia.

transition temperature of sPS (100 °C), co-crystalline phases between the polymer and the low molecular weight guest molecules are formed, where the polymer exhibits the *TTGG* conformation. If the guest molecules are completely removed by, for example, supercritical carbon dioxide, the resulting sPS will have a completely empty δ-form crystal [15]. The δ-form sPS is a nanoporous metastable polymorph including centrosymmetric crystalline cavities of about 120–160 Å^3 [16].

When a dilute solution of sPS is crystallized at low temperature (below 100 °C), sPS gels develop in the form of long nanofibrils of about 30–100 nm diameter [8,9,17–23]. It has been suggested that the fibrous and network morphology of sPS is induced by the mobile solvent molecules that disturb the isotropic growth of polymer crystals into a three-dimensional structure [8]. The polymer–solvent interaction affects the morphology of sPS gels. For example, sPS/*trans*-decalin gels, albeit with a structure consisting of a polymer–solvent compound with 2_1-helix form, do not show a fibrous and network morphology but exhibit a spherulitic morphology [18]. The potential applications of fibrillar networks as well as the microporous structures of sPS include membranes for the purification of water contaminated by organic chemicals [24,25], sPS aerogels for insulations and catalysis [19,22,26], chemical sensors [27–29], and gas storage media [30].

Although there are many reports on the thermoreversible gelation and crystallization of sPS from a dilute solution, little has been reported on the morphology of sPS during the polymerization with heterogeneous metallocene catalysts. In this study, we have investigated the morphology of sPS synthesized over silica-supported metallocene catalyst in a liquid slurry polymerization process. We report new and interesting findings from our experimental study.

2. Experimental

2.1. Materials

Styrene (Aldrich) was vacuum distilled over calcium hydride, and activated alumina was used to remove inhibitor (4-*tert*-butylcatechol) from styrene. *n*-Heptane (Fisher Scientific) used as a diluent was purified by being refluxed over sodium and benzophenone. The metallocene catalyst, Cp*Ti(OCH$_3$)$_3$ (pentamethyl cyclopentadienyl titanium trimethoxide) (Strem Chemical), and modified methyl aluminoxane (MMAO, Akzo Nobel) were used as supplied without further purification. We used two silica gels with different average pore sizes (Davison 952, W.R. Grace, average pore diameter: 20 nm; Davisil™ 633, Sigma Aldrich, average pore size: 6 nm) to support the metallocene catalysts. The silica particle size ranges from ca. 30 to 100 μm.

2.2. Preparation of silica-supported metallocene catalysts

Silica gel particles were calcined in an oven at 250 °C for 24 h under nitrogen atmosphere. The calcined silica particles were treated with MMAO solution (8.0×10^{-3} mol Al in toluene) at 50 °C for 1.5 h, washed with excess toluene three times, and dried in vacuo overnight. Then, the MMAO/silica particles were mixed with Cp*Ti(OCH$_3$)$_3$ catalyst solution (1.5×10^{-3} mol Ti in toluene) at 50 °C for 1 h, washed with toluene three times, and dried in vacuo for 24 h. The Al and Ti loadings measured by inductively coupled plasma emission spectroscopy (ICP) were 1.30×10^{-3} mol Al/g catalyst and 2.92×10^{-4} mol Ti/g catalyst, respectively. Fig. 1(a) shows a scanning electron microscopic (SEM) image of the Davison 952 silica surface used in this study. As is known, we can see in Fig. 1(a) that the silica support consists of multilevel aggregates of 2–10 nm diameter primary silica particles [31,32]. The primary silica particles or spheroids are formed during the polymerization of silicic acid solution and the subsequent aggregation of colloidal
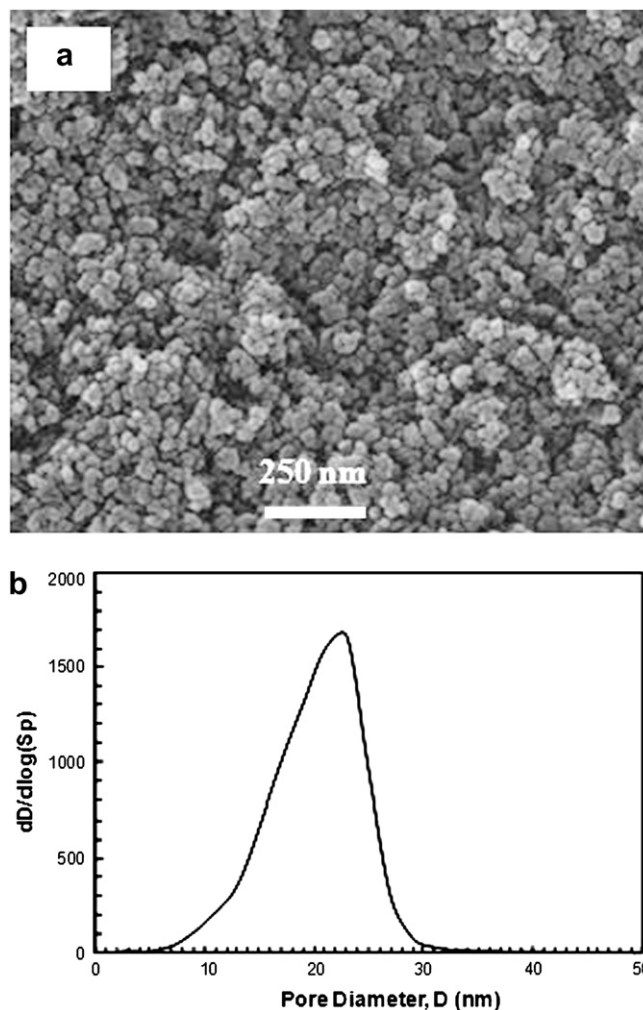

Fig. 1. (a) SEM image of Davison 952 silica gel particle and (b) the pore size distribution (Courtesy of W.R. Grace and Company).

silica. These spheroids aggregate and form larger clusters. The pores for the diffusion of monomer and the growth of polymers are provided by the channels between the primary particles and the channels between the clusters. Fig. 1(b) is the pore size distribution of the Davison 952 silica particles [Courtesy of W.R. Grace and Company, Columbia, MD]. The average pore diameter is 20 nm and the pores larger than 30 nm are practically absent.

2.3. Polymerization

Styrene polymerization experiments were carried out in a jacketed glass reactor (100 mL). The reactor was first charged with predetermined amounts of purified monomer, *n*-heptane, supported catalyst, and MMAO under argon atmosphere. The reactor was fitted with a magnetically sealed agitator assembly in a glove box. All the polymerization experiments were carried out at 70 °C, and the agitator speed was maintained constant during the polymerization. The polymerization temperature was controlled by circulating hot water in an outer jacket of the glass reactor. After polymerization, the reaction mixture was discharged from the reactor, washed with excess amount of acidified methanol (10 vol.% of hydrochloric acid), and dried in vacuo. The monomer conversion was determined gravimetrically. We carried out polymerization experiments at several different initial styrene volume fractions: 0.10, 0.25, 0.40, and 0.60. The activity of the silica-supported catalyst is in the range from 0.16×10^3 Kg/mol Ti h to 1.10×10^3 Kg/mol

Table 1
Experimental sPS polymerization data

Run ID	[Ti] $\times 10^4$ [mol/L]	St. [vol. %]	$[M]_0^a$ [mol/L]	Time [min]	Conv. [%]	X_c^b [%]	T_m^c [°C]	MEK insoluble [%]	Catalyst activity [Kg sPS/mol Ti h]
20-1	2.62	10	0.81	10	26.5	24.2	270.7	95.9	514.8
20-2	2.62	10	0.81	60	49.4	40.0	270.1	91.1	159.0
20-3	2.62	25	2.02	10	22.6	26.9	269.7	98.4	1093.2
20-4	2.62	25	2.02	60	43.7	43.5	269.5	95.1	352.8
20-5	2.62	60	4.86	10	9.5	29.8	270.2	97.0	1104.0
20-6	2.62	60	4.86	60	31.0	40.0	269.7	94.6	468.6
20-7	3.95	60	4.71	2	4.04	–	–	–	912.0
6-1	1.73	40	3.24	30	6.95	–	–	90.9	282.0

60 mL (Run ID: 20-1 to 20-6, 6-1), 10 mL (Run ID: 20-7) of styrene and *n*-heptane were used; [Al]/[Ti] = 500, average pore size of silica gel = 20 nm (Run ID: 20-1 to 20-7), 6 nm (Run ID: 6-1).

  [a] Initial monomer concentration (mol/L).
  [b] Degree of crystallinity.
  [c] Melting temperature (°C).

Ti h. The methyl ethyl ketone (MEK) insoluble fraction is generally used as a quick but approximate measure of the syndiotacticity. Most of the sPS samples obtained in our experiments had the MEK insoluble fraction of 91–98%, indicating high degree of syndiotacticity. Table 1 is a summary of the experimental reaction data. In our experiments, the same batch of catalyst was used to minimize the run-to-run variations in catalyst activity.

2.4. Polymer analysis

The morphology of the polymer was investigated by scanning electron microscopy (SEM) using Hitachi S-4700 and SU-70. The sPS samples were coated with AuPd layer of thickness 5 nm in a Denton DV-503 vacuum evaporator coating apparatus (Denton Ltd.). The polymer crystallinity and melting points were measured by differential scanning calorimetry (DSC) with a heating rate of 20 °C/min under nitrogen gas flow using Q100 System (TA Instruments). EDAX (Ametek) attached to AMRAY-1610 was used for energy dispersive X-ray spectroscopic (EDX/EDS) analysis of sPS. X-ray diffraction (XRD) patterns were obtained by D4 ENDEAVOR diffractometer (Bruker AXS Inc.) with Cu Kα as a radiation source in the range of 5°–30° of 2θ. Thermogravimetric analysis (TGA) was performed in the temperature range of 30–550 °C at a heating rate of 10 °C/min under nitrogen atmosphere (nitrogen flow rate: 100 mL/min) using 2050 TGA system (TA Instruments).

3. Results and discussion

3.1. Particle morphology

To observe the nascent morphology of sPS at its early stage, a polymer sample was taken 2 min after polymerization at the
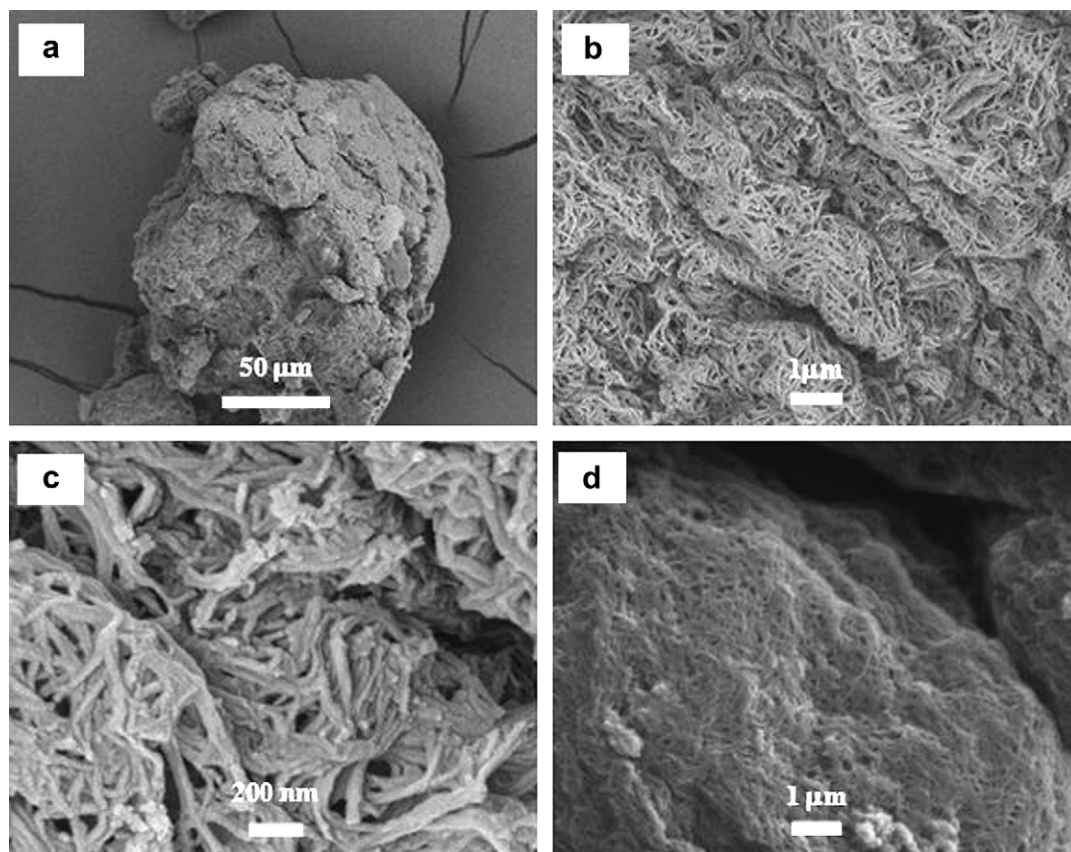

Fig. 2. SEM images of sPS particle produced over silica-supported Cp*Ti(OCH₃)₃/MAO catalyst in *n*-heptane: pore size of silica gel = 20 nm; (a)–(c) [M]₀ = 4.71 mol/L, reaction time = 2 min, Run ID: 20-7; (d) [M]₀ = 4.86 mol/L, reaction time = 10 min, Run ID = 20-5.

initial styrene concentration of 4.71 mol/L. Since the catalyst activity is very high, the monomer conversion reached 4.0% at 2 min and it corresponds to the total solid content (TSC) of 2.67%. When the sample was taken, the polymerization mixture was a turbid slurry of polymer particles. Fig. 2(a) illustrates a large 100–120 μm sPS particle sample. The exterior surface of the particle is very rough and it appears that the particle is an agglomerate of irregularly shaped and smaller subparticles. The close-up images of the polymer particle surface shown in Fig. 2(b) and (c) reveal interesting polymer morphologies. Notice that the sPS particle surface is covered with heavily entangled long nanofibrils of 30–50 nm in diameter. Although it is difficult to measure the exact lengths of the nanofibrils from the SEM images, these nanofibrils appear to be quite long and rigid. Fig. 2(d) shows the polymer sample taken at 10 min of reaction time. The surface morphology of the particle is same as seen in Fig. 2(a)–(c).

The fibrillar morphology of sPS shown in Fig. 2 is very different from the granular particle morphology commonly observed in polyolefins synthesized over heterogeneous Ziegler–Natta catalysts or silica-supported catalysts [33–36]. In polyolefin processes, the fragmentation of catalyst supports leads to the exposure of active catalytic sites to monomers for high activity and the fragmented catalyst particles grow to larger polymer particles. Several morphological models for olefin polymerization have been proposed in the literature with the multigrain model as the most well known and accepted [37,38].

To observe the interior structure of a polymer particle, we mechanically fractured an sPS particle sample taken at 10 min of reaction (Fig. 3(a): Run ID 20-5). Fig. 3(b) shows the close-up view of the cross-section of the fractured polymer particle. The most prominent feature of the polymer morphology revealed in Fig. 3(b) is that the particle interior is densely packed with

polymer nanofibrils of quite uniform diameter (ca. 30–50 nm). The dimension of these nanofibrils is the same as that observed at the particle surface (Fig. 2). Since the polymer particle is packed with thin and long nanofibrils, the particle interior seems to have a large fraction of void space. In our previous study [10], we found that 1 g of nascent sPS particles polymerized over the same silica-supported catalyst can absorb more than 6 mL of solvent (*n*-heptane). The interior morphology of the sPS particle shown in Fig. 3(b) suggests that the nanofibrillar growth is probably responsible for such a high solvent absorbability of sPS particles. It is also interesting that the nanofibrils inside the particle are not entangled but rather straight and separated from each other. Fig. 3(c) shows the edge portion of the fractured particle surface and Fig. 3(d) is the close-up view of the particle surface. It is seen in both Fig. 3(c) and (d) that the nanofibrils grow out from the particle interior and they collapse and fuse at the particle surface as they are exposed to the bulk liquid phase during the polymerization. The shear force exerted by agitation in the reactor might have also promoted the adhesion of sPS nanofibrils at the surface, making them look like a fused layer.

To investigate the effect of the pore size of silica gel on the dimension of sPS nanofibrils, we carried out polymerization experiments with the catalyst supported on the silica gel with smaller pore diameter (Davisil™ 633, average pore size: 6 nm). Fig. 4 shows the interior morphology of a polymer particle. Again, we can see that the particle interior is densely packed with nanofibrils of 30–50 nm diameter, which is very similar to that observed with Davison 952 catalyst support having much larger average pore diameter (20 nm). Fig. 4(b) shows that some polymer fibrils are as thin as about 10–15 nm and some nanofibrils aggregate to larger-diameter bundles. The results shown in Figs. 2–4 indicate that the
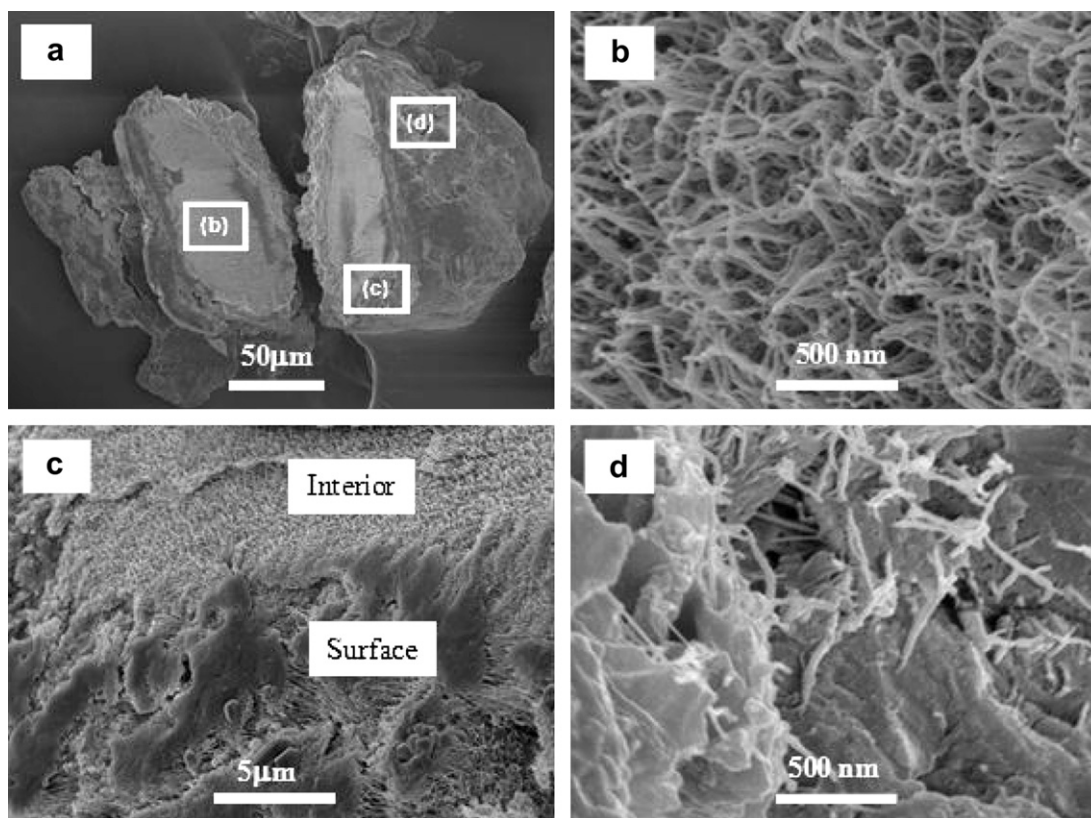

Fig. 3. SEM images of sPS particle's cross-sections: pore size of silica gel = 20 nm, [M]$_0$ = 4.86 mol/L, T = 70 °C, reaction time = 10 min, Run ID = 20-5; (a) fractured sPS particle, (b) particle interior, (c) edge portion of the sPS particle, and (d) close-up of the particle surface.
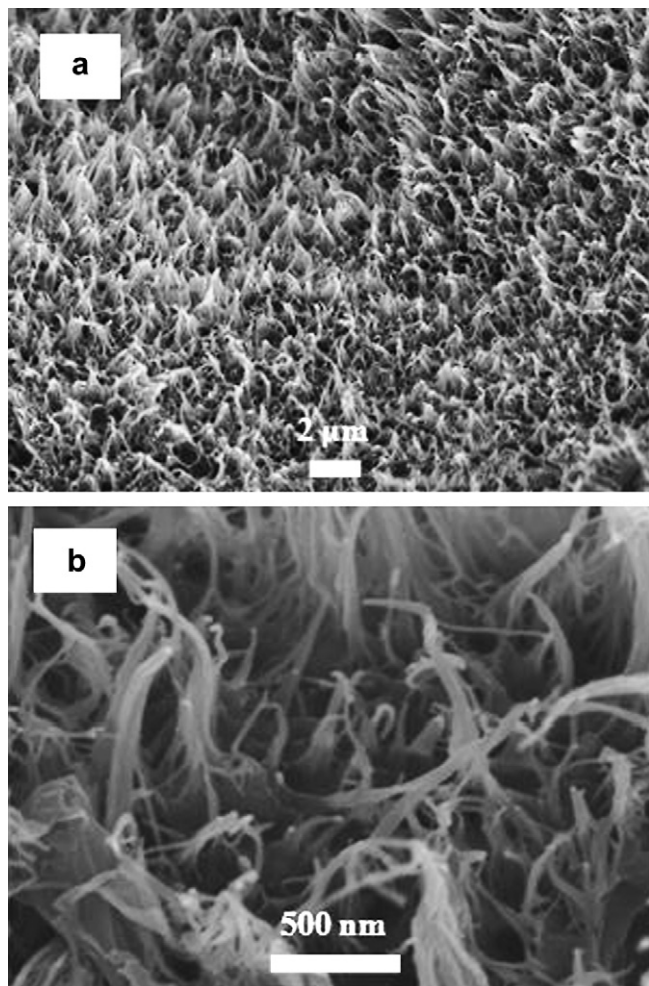
Fig. 4. (a) SEM images of sPS produced over silica-supported Cp*Ti(OCH₃)₃/MAO catalyst having smaller pore size, close-up view: pore size of silica gel = 6 nm, $[M]_0 = 3.24$ mol/L, reaction time = 30 min, Run ID = 6-1.

silica pore size has no effect on the diameter of sPS nanofibrils. In other words, the sPS nanofibrils are the intrinsic morphology of the polymer.

3.2. Crystalline structure of sPS

sPS has four main polymorphs (i.e., α, β, γ, δ forms) that differ with respect to the chain conformation and the chain packing within the unit cell [7]. The α and β forms have the sPS chains in the *trans*-planar, zigzag conformation, while the γ and δ forms have a 2_1-helix conformation. When a thin layer of sPS melt is slowly cooled to room temperature, the polymer crystallizes in lamellar or spherulite morphology to a mixture of α and β forms of crystals [39–42]. However, when sPS is crystallized by solvent-induced crystallization, δ-form crystal is obtained. In a typical crystallization
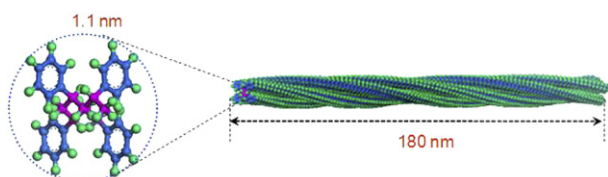

Fig. 5. 2_1-Helix of a single sPS chain with 1000 styrene units: drawing based on Materials Studio® modeling package (Accelrys Software Inc.).
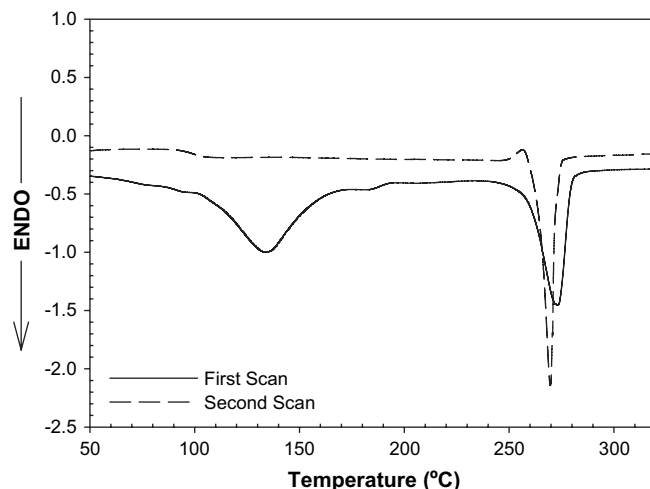

Fig. 6. DSC thermograms of the sPS polymerized with silica-supported Cp*Ti(OCH₃)₃/MAO catalyst: pore size of silica gel = 20 nm, $[M]_0 = 4.86$ mol/L, reaction time = 60 min, Run ID = 20-6.
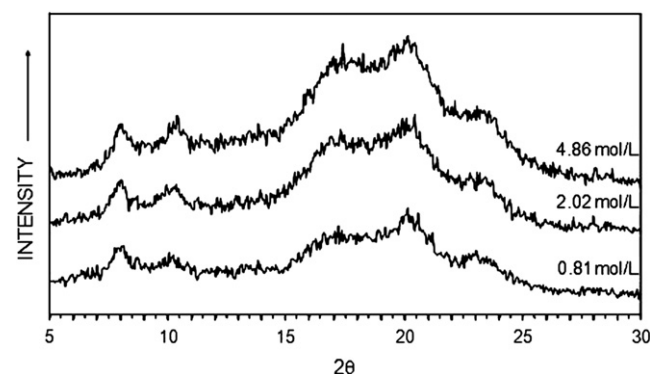

Fig. 7. XRD patterns of sPS particles synthesized over silica-supported Cp*Ti(OCH₃)₃/MAO catalyst in *n*-heptane: pore size of silica gel = 20 nm, reaction time = 60 min.

experiment, a homogeneous solution of sPS dissolved in a solvent at high temperatures is cooled to lower temperatures, leading to the formation of thermoreversible gels of fibrillar network
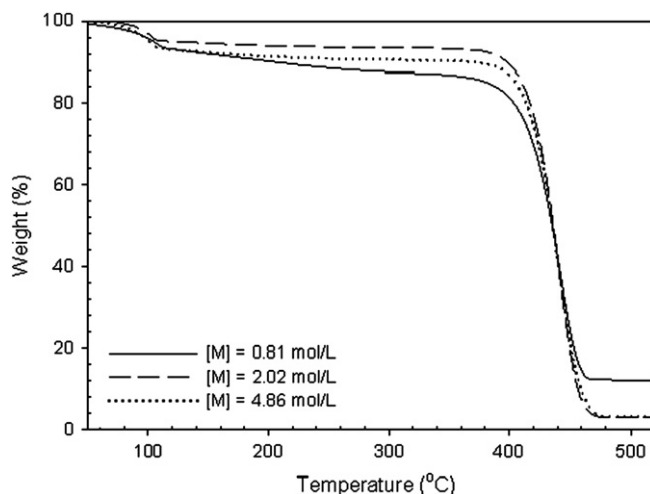

Fig. 8. TGA thermograms of nascent sPS samples synthesized over silica-supported Cp*Ti(OCH₃)₃/MAO catalyst in *n*-heptane: pore size of silica gel = 20 nm, reaction time = 60 min.
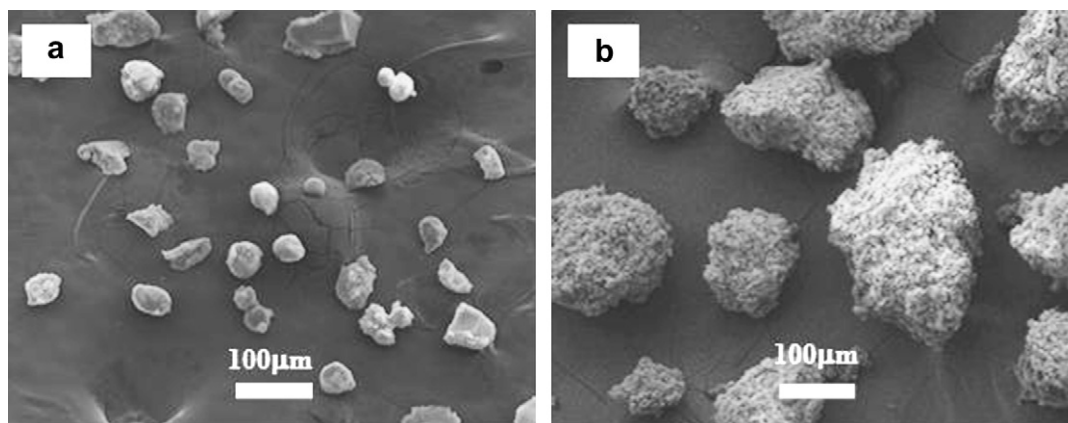
Fig. 9. SEM images of silica gel and sPS particles: (a) Davison 952 silica gel and (b) polymerized sPS particles, $[M]_0 = 2.02$ mol/L, reaction time = 60 min, Run ID = 20-4.

structure or paste-like systems with spherulites [17]. The solvent does not bind with the sPS chains but acts as a solvating agent to cause the formation and stabilization of helical chains.

The formation of δ-form crystal or co-crystal is also related to the formation of nanofibrils because the sPS chain rigidity increases with a strong interaction between polymer chain (host)
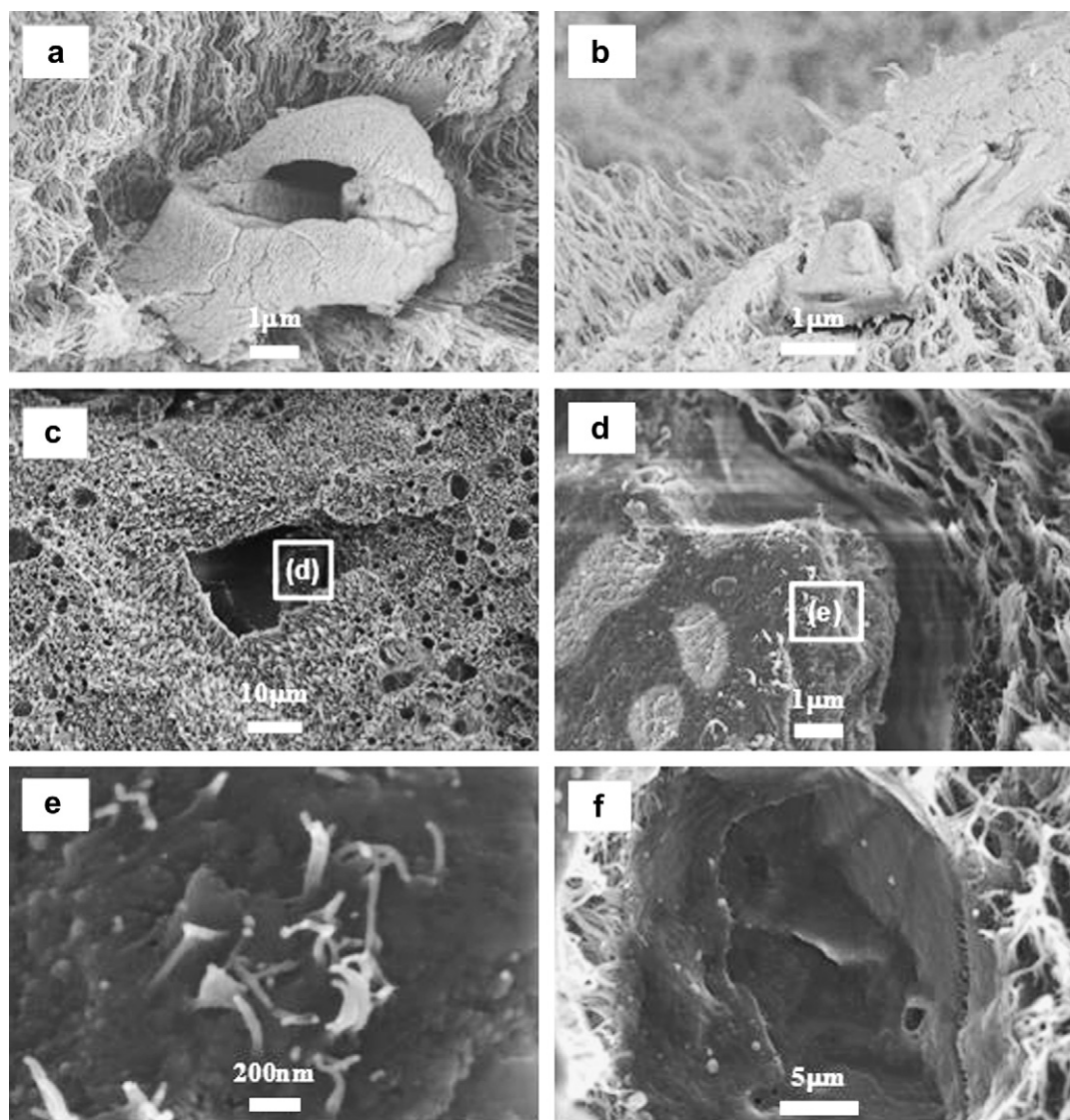

Fig. 10. SEM images of fractured sPS particles: (a) and (b) pore size of silica gel = 20 nm, $[M]_0 = 4.71$ mol/L, reaction time = 2 min, Run ID = 20-7; (c)–(f) pore size of silica gel = 6 nm, $[M]_0 = 3.24$ mol/L, reaction time = 30 min, Run ID = 6-1.

and solvent molecules (guest), leading to an increased correlation length [22]. δ-Form sPS crystal is nanoporous with its cavity volume to be about 120 Å^3 and has a density (0.977 g/cm^3) lower than amorphous sPS (1.04 g/cm^3) [43,44]. Fig. 5 shows a single δ-form sPS chain of a 2_1-helix conformation with 1000 styrene units (MW = 104,000) constructed by using Materials Visualizer (Accelrys Software Inc.). The diameter of the polymer chain is 1.1 nm. Using the unit cell dimension of a δ-form sPS crystal (a = 17.47 Å, b = 13.42 Å) [43,45], we can calculate that about 350 sPS polymer chains are needed to constitute the diameter of a single sPS fibril of 30 nm observed by SEM. Since the length of sPS nanofibrils observed in the previous SEM images is quite larger than the length of a single sPS chain (e.g., 180 nm for MW = 104,000, 1.8 μm for MW = 1,040,000), we can say that the observed sPS nanofibrils are the aggregates of a large number of polymer chains grown from the active catalyst sites in the direction of fibrillar growth. The nanoporous δ-form sPS can rapidly absorb certain organic compounds and form the clathrates. With the clathration, the unit cell of the δ-form is enlarged and the cavity can include molecules larger than its original size [46,47].

Fig. 6 shows the DSC thermograms of the sPS synthesized over silica supported catalyst. There are two melting endotherms in the first scan. The broad first melting endotherm at about 130–150 °C corresponds to the transformation of the δ-form crystals to the γ-form crystals [7]. In this temperature range, the solvent molecules are removed from the sPS particles. The melting endotherm at about 270 °C corresponds to the melting of the α-form crystals of sPS. The second scan shows the glass transition point at 100 °C. Since the sPS sample has been transformed into α-form sPS crystal during the first scan, no crystalline melting peak is observed at 130–150 °C in the second scan thermogram. The melting point in the second scan is slightly lower than the melting point in the first scan. The degree of crystallinity of sPS samples in our experiments is 24–44%.

The XRD patterns of sPS polymerized over silica-supported metallocene catalyst are shown in Fig. 7 for the three polymers at three different initial monomer concentrations. Before the X-ray diffraction analysis, the nascent sPS samples were dried in vacuo overnight at ambient temperature. All these XRD patterns show that these polymers are the co-crystals or filled δ-form crystals of sPS clathrated with the residual monomer styrene or n-heptane (diluent) as characterized by the peaks at $2\theta \approx 8$, and 10.5° [15,43,48]. The thermogravimetric analysis (TGA) shown in Fig. 8 indicates 5–8% weight loss of the sPS samples at 80–120 °C, confirming the presence of low molecular weight guest molecules co-crystallized with sPS. The DSC and XRD data show that the crystalline structure of the sPS particles polymerized over silica-supported Cp*Ti(OCH$_3$)$_3$/MAO catalyst is very similar to those of the thin sPS films crystallized by solvent induced crystallization technique as reported in the literature.

3.3. Macroscopic growth of sPS particles

During the slurry phase polymerization of styrene, the size of sPS particles increases. Fig. 9(a) and (b) shows the SEM micrographs of Davison 952 silica gel particles (average pore size of 20 nm) and the polymerized sPS particles produced after 60 min, respectively. We can see that the size of the original catalyst-supported silica gel particles is about 30–100 μm and the sPS particles have grown to about 100–300 μm diameter. It is also interesting to observe that the fully grown sPS particles seem to have replicated the shapes of the original silica particles. Although the particle's interior morphology of sPS is quite different from that of polyolefins (e.g., globular), Fig. 9 suggests
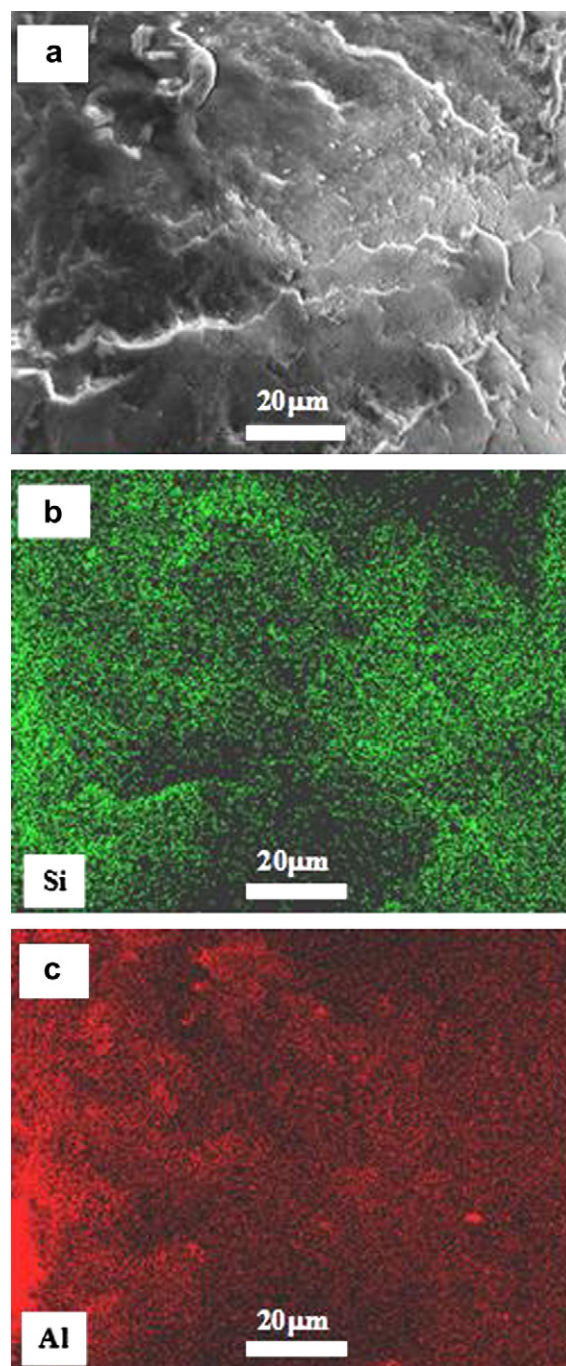

Fig. 11. Element distribution mappings of a fractured sPS particle produced over silica-supported Cp*Ti(OCH$_3$)$_3$/MAO catalyst: pore size of silica gel = 20 nm, [M]$_0$ = 4.86 mol/L, reaction time = 10 min, Run ID = 20-5: (a) SEM image, (b) Si mapping, and (c) Al mapping.

that the 'shape replication' phenomena commonly observed in heterogeneous α-olefin polymerization processes also occur in sPS polymerization with silica-supported catalysts. The uniform dispersion of catalyst in the original catalyst and the uniform growth of sPS nanofibrils in a polymer particle with silica fragmentation are believed to be the reason for such shape replication phenomena.

Before we consider the sPS particle growth mechanism during the polymerization, let us briefly review the particle growth phenomena observed in ethylene or propylene polymerization over silica-supported chromium oxide or metallocene catalysts.

The silica particle fragmentation and the development of polymer particle morphology in olefin polymerization are most succinctly described by Fink and coworkers [49,50]: Initially, a thin polymer shell is formed on the silica particle surface. The polymer shell creates a diffusion barrier for monomer. As polymerization continues, the buildup of hydraulic forces in the particle pores increases, leading to the fragmentation of the silica support from the particle surface to the interior. New active centers are exposed by the fragmentation for increased rate of polymerization. The ultimate catalyst fragment size is about 20–100 nm, which is also an agglomerate of smaller primary silica particles of about 5–10 nm. Each fragmented particle is encapsulated in polymer and tied to its neighbor through polymer entanglements [51].

Fig. 10 shows several SEM images of the sPS particle interior. In Fig. 10(a), we can see a silica particle fragment of about 5–6 μm diameter embedded in a densely populated sea of sPS nanofibrils. In some edge portion of the unfragmented silica particle, sPS nanofibrils are attached to the silica surface, suggesting that sPS chains grow at the catalytic sites anchored onto a silica surface. The lack of sPS nanofibrils on the silica particle surface in Fig. 10(a) might have been caused by the absence of catalyst or no particle fragmentation.

Fig. 10(b) shows the unfragmented silica particles at a different location in the polymer particle sample. Notice that the exposed silica top surface has no polymer fibrils whereas the bottom part of the silica clearly shows the sPS nanofibrils growing from the surface of the silica where active catalyst sites are expected to be present. Fig. 10(c) shows an interesting cross-sectional view of another polymer particle. There is a large cavity in the center which is believed to be left by a silica particle removed during the sample fracture. Around the large cavity, we can also see many smaller cavities (circular shape) that might have also been left by smaller silica particles removed during the sample fracture.

Fig. 10(d) is the close-up image of the large cavity in Fig. 10(c). We can see that another silica particle is embedded underneath surrounded by sPS nanofibrils. It is also seen that the silica particle surface has several lighter regions where few polymer fibrils are visible. If we carefully observe the surface texture of the 'bare' silica particle in Fig. 10(d), we can see the original silica micrograins as observed in Fig. 1(a). No reaction might have occurred in these bare regions. Interestingly, a similar SEM image was reported for a silica-supported chromium oxide catalyst for gas phase ethylene polymerization [31]. Fig. 10(e) is a close-up view of the edge portion of the embedded silica particle in Fig. 10(d). It shows that sPS nanofibrils formed inside the void between the silica aggregates are extruding out or sPS nanofibrils are growing from the silica surface. Fig. 10(f) is a close-up image of another empty cavity left by a large silica particle fragment. It appears that some part of the original silica fragment is still present because the sPS nanofibrils growing from the particle surface are holding the particle.

We also analyzed the polymer particle by EDX analysis to examine how the fragmented silica particles are distributed in an sPS particle. Fig. 11(a) shows the SEM image of a cut surface of an sPS particle and Fig. 11(b) and (c) shows the silicon and aluminum mapping. It is seen that both silicon and aluminum are quite homogeneously dispersed in the polymer, suggesting that the fragmentation of MAO-activated silica-supported metallocene catalyst has occurred with the particle expansion.
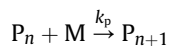
3.4. Polymer particle growth mechanism

The growth of sPS over silica-supported Cp*Ti(OCH$_3$)$_3$/MAO catalyst can be described by the following single-site reaction model [10]:
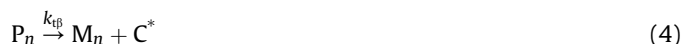
Catalyst site activation:

$$C_0 + MAO \xrightarrow{k_a} C^* \tag{1}$$

Chain propagation:

$$C^* + M \xrightarrow{K_p} P_1 \tag{2}$$

$$P_n + M \xrightarrow{k_p} P_{n+1}$$

Chain transfer to monomer:

$$P_n + M \xrightarrow{k_{tM}} M_n + P_1 \tag{3}$$

β-Hydrogen elimination:

$$P_n \xrightarrow{k_{t\beta}} M_n + C^* \tag{4}$$

where C_0 is the potent catalyst site, C^* is the activated catalyst site, P_n and M_n are the live and dead polymer chains of length n, and M is the monomer. The dead polymer chains are formed through both chain transfer to monomer and β-hydrogen elimination reactions. The chain propagation and chain transfer reactions are the major reactions that determine the chain lengths of sPS molecules. The turnover frequency (TOF) is defined as the number of molecules of monomer that converts to polymer chain per catalytic site per unit time. The TOF can be calculated from polymerization rate as follows:

$$TOF = \frac{R_p}{[C^*]_t} \tag{5}$$

where $[C^*]_t$ is the total active site concentration. From the experimental catalyst activity data shown in Table 1, we can estimate the TOF of the silica-supported catalyst. If we assume that all the titanium sites are active, the TOF value is about 1–3 styrene molecules per Ti site per second. If a comparison is made with MgCl$_2$-supported TiCl$_x$ catalysts for propylene polymerization, the TOF for propylene polymerization is estimated to be about 30–60 C$_3$H$_6$ molecules per second if the number of active sites is 10% of the surface titanium ions [52]. If the number of active sites in the silica-supported catalyst used in our study is also only 10%, the TOF for sPS polymerization will be 10–30, which is quite comparable to that of polypropylene catalysts. The fraction of active titanium sites can be even lower than 10%.

The crystallization rate of sPS in solvent vapor induced crystallization has been reported to be fast and hence, limited by solvent vapor diffusion through a solid sPS matrix [14,53]. In our polymerization system, such monomer or solvent diffusion resistance is not expected to be present because the polymerization occurs in the solid phase saturated with the liquid monomer and solvent. Since the TOF value estimated from the polymerization kinetic data is not very large, we expect that the sPS co-crystallizes as soon as it is formed at the catalyst site and both styrene/heptane molecules and sPS chain have sufficient time to intercalate. As a result, the polymer chains can easily form rigid nanofibrils.

From the foregoing SEM and EDX analyses, we can propose a following particle forming and growth mechanism. In a liquid phase slurry polymerization of styrene with silica-supported catalyst, monomer and solvent penetrate into silica gel pores and monomer polymerizes at the surface of silica micrograins. As sPS is formed, it rapidly crystallizes in the presence of monomer and

solvent molecules. The sPS-monomer/solvent intercalates are rigid and the polymer grows as a thin nanofibril. The nanofibrils from the neighboring active catalyst sites quickly self-assemble to a bundle of nanofibrils of larger diameter of about 30 nm. As these bundles of nanofibrils fill up the void space, a buildup of hydraulic pressure occurs within the catalyst particle and eventually leading to the disintegration of the primary silica particles. Then the expanded void space between the fragmented silica particles is filled up with growing sPS nanofibrils. Since the fibrillar morphology offers a large void space, monomer transport resistance from the bulk liquid phase to the polymer particle is expected to be very small. As a result, the entire polymer particle grows with a uniform interior morphology created by the uniform sized sPS nanofibrils. Also, some nanofibrils can intertwine and form larger fibrils. Finally, polymer particles continue to expand as more sPS fibrils are produced. The sPS fibrils at the surface of the particle are exposed to the liquid phase and the shear stress by mechanical agitation. Then, they collapse and stack themselves like a fused layer. When the reaction time is very short (e.g., 2–10 min), the sPS fibrils at the surface still maintain their fibrillar structures but at longer reaction times, such fibrillar structure is hard to see at the particle surface because the fibrils are exposed to the liquid phase too long and they deform.

4. Concluding remarks

In this study, we have reported the morphology and crystalline structure of sPS particles synthesized over silica supported $Cp^*Ti(OCH_3)_3$ catalyst with MMAO. The scanning electron microscopic analysis of the nascent sPS synthesized over a silica-supported catalyst reveals that the morphology of the sPS particles is characterized by the nanofibrillar morphology with extensive silica particle fragmentation. Our experimental data also indicate that the dimension of sPS nanofibrils (30–50 nm) is independent of the silica pore size. The XRD analysis shows that the sPS obtained in a liquid slurry polymerization experiments is the co-crystal. The degree of crystallinity of the polymer is in the range of 24–44%. From the SEM and EDX analyses, we observed that fragmentation of silica particles has occurred during the polymerization. Although the sPS particle growth is through nanofibrils, the experimental observations indicate that the particle shape replication also occurs in a silica supported sPS polymerization. Based on the observations in our study, we have proposed a mechanism for the growth of sPS particles.

References

[1] Malanga M. Adv Mater 2000;12(23):1869–72.
[2] Schellenberg J, Leder HJ. Adv Polym Technol 2006;25(3):141–51.
[3] Ishihara N, Seimiya T, Kuramoto M, Uoi M. Macromolecules 1986;19(9):2464–5.
[4] Ishihara N, Kuramoto M, Uoi M. Macromolecules 1988;21(12):3356–60.
[5] Choi KY, Chung JS, Woo BG, Hong MH. J Appl Polym Sci 2003;88(8):2132–7.
[6] Chung JS, Woo BG, Choi KY. Macromol Symp 2004;206:375–82.
[7] Guerra G, Vitagliano VM, Derosa C, Petraccone V, Corradini P. Macromolecules 1990;23(5):1539–44.
[8] Itagaki H, Mochizuki J. Macromolecules 2005;38(23):9625–30.
[9] Malik S, Rochas C, Guenet JM. Macromolecules 2005;38(11):4888–93.
[10] Han JJ, Lee HW, Yoon WJ, Choi KY. Polymer 2007;48(22):6519–31.
[11] Lee HW, Chung JS, Choi KY. Polymer 2005;46(14):5032–9.
[12] Prasad A, Mandelkern L. Macromolecules 1990;23(23):5041–3.
[13] Daniel C, Dammer C, Guenet JM. Polymer 1994;35(19):4243–6.
[14] Tashiro K, Yoshioka A. Macromolecules 2002;35(2):410–4.
[15] Reverchon E, Guerra G, Venditto V. J Appl Polym Sci 1999;74(8):2077–82.
[16] Tarallo O, Petraccone V, Venditto V, Guerra G. Polymer 2006;47(7):2402–10.
[17] Ray B, Elhasri S, Thierry A, Marie P, Guenet JM. Macromolecules 2002;35(26):9730–6.
[18] Malik S, Rochas C, Schmutz M, Guenet JM. Macromolecules 2005;38(14):6024–30.
[19] Daniel C, Alfano D, Venditto V, Cardea S, Reverchon E, Larobina D, et al. Adv Mater 2005;17(12):1515–8.
[20] Malik S, Rochas C, Guenet JM. Macromolecules 2006;39(3):1000–7.
[21] Malik S, Roizard D, Guenet JM. Macromolecules 2006;39(18):5957–9.
[22] Daniel C, Avallone A, Guerra G. Macromolecules 2006;39(22):7578–82.
[23] Guenet JM. Macromol Symp 2006;241:45–50.
[24] Guerra G, Milano G, Venditto V, Musto P, De Rosa C, Cavallo L. Chem Mater 2000;12(2):363–8.
[25] Mahesh KP, Sivakumar M, Yamamoto Y, Tsujita Y, Yoshimizu H, Okamoto S. J Polym Sci Part B Polym Phys 2004;42(18):3439–46.
[26] Daniel C, Sannino D, Guerra G. Chem Mater 2008;20(2):577–82.
[27] Giordano M, Russo M, Cusano A, Cutolo A, Mensitieri G, Nicolais L. Appl Phys Lett 2004;85(22):5349–51.
[28] Giordano M, Russo A, Cusano A, Mensitieri G. Sens Actuators B Chem 2005;107(1):140–7.
[29] Giordano M, Russo M, Cusano A, Mensitieri G, Guerra G. Sens Actuators B Chem 2005;109(2):177–84.
[30] Annunziata L, Albunia AR, Venditto V, Mensitieri G, Guerra G. Macromolecules 2006;39(26):9166–70.
[31] Niegisch WD, Crisafulli ST, Nagel TS, Wagner BE. Macromolecules 1992;25(15):3910–6.
[32] Ullmann's encyclopedia of industrial chemistry. 1st ed. Wiley; 1993.
[33] Ferrero MA, Chiovetta MG. Polym Eng Sci 1987;27(19):1436–47.
[34] Kakugo M, Sadatoshi H, Sakai J, Yokoyama M. Macromolecules 1989;22(7):3172–7.
[35] Estenoz DA, Chiovetta MG. Polym Eng Sci 1996;36(17):2208–28.
[36] Estenoz DA, Chiovetta MG. J Appl Polym Sci 2001;81(2):285–311.
[37] Hutchinson RA, Chen CM, Ray WH. J Appl Polym Sci 1992;44(8):1389–414.
[38] Debling JA, Ray WH. Ind Eng Chem Res 1995;34(10):3466–80.
[39] Sun YS, Woo EM. J Polym Sci Part B Polym Phys 2000;38(24):3210–21.
[40] Sun YS, Woo EM. Polymer 2001;42(5):2241–5.
[41] Woo EM, Sun YS, Yang CP. Prog Polym Sci 2001;26(6):945–83.
[42] Wang C, Lin CC, Chu CP. Polymer 2005;46(26):12595–606.
[43] De Rosa C, Guerra G, Petraccone V, Pirozzi B. Macromolecules 1997;30(14):4147–52.
[44] Larobina D, Sanguigno L, Venditto V, Guerra G, Mensitieri G. Polymer 2004;45(2):429–36.
[45] Tamai Y, Fukuda M. Polymer 2003;44(11):3279–89.
[46] Milano G, Venditto V, Guerra G, Cavallo L, Ciambelli P, Sannino D. Chem Mater 2001;13(5):1506–11.
[47] Rizzo P, Lamberti M, Albunia AR, de Ballesteros OR, Guerra G. Macromolecules 2002;35(15):5854–60.
[48] Rani DA, Yamamoto Y, Saito A, Sivakumar M, Tsujita Y, Yoshimizu H, et al. J Polym Sci Part B Polym Phys 2002;40(6):530–6.
[49] Fink G, Steinmetz B, Zechlin J, Przybyla C, Tesche B. Chem Rev 2000;100(4):1377–90.
[50] Knoke S, Ferrari D, Tesche B, Fink G. Angew Chem Int Ed 2003;42(41):5090–3.
[51] Wagner BE, Niegisch WD. Polym Mater Sci Eng 1991;64:139–41.
[52] Kim SH, Somorjai GA. Proc Natl Acad Sci USA 2006;103(42):15289–94.
[53] Gupper A, Chan KLA, Kazarian SG. Macromolecules 2004;37(17):6498–503.